



Cite this: *Polym. Chem.*, 2016, 7, 2858

# Versatile procedure for site-specific grafting of polymer brushes on patchy particles *via* atom transfer radical polymerization (ATRP)†

Bas G. P. van Ravensteijn\* and Willem K. Kegel\*

We report the preparation of chemically anisotropic colloidal dumbbells of which one lobe is functionalized with chemical handles in the form of chlorine groups. The chlorines are easily converted to azides and subsequently to active initiators for Atom Transfer Radical Polymerization (ATRP) by Click Chemistry. These initiators are exploited for site-specific grafting of poly(*N*-isopropylacrylamide) (p(NIPAM)) brushes on the reactive patches. The geometric ratio between the grafted and non-grafted lobe is tunable by the shape of the initial dumbbell and the polymer grafting time. Furthermore, the versatility of our synthesis protocol is underlined by extending it to colloids with multiple reactive patches. The partially grafted dumbbell-shaped particles are employed as building blocks for finite-sized colloidal clusters. A directional interaction between the non-grafted lobes is easily introduced by dispersing the partially grafted dumbbells in a high ionic strength medium. Finally, we briefly explore the potency of this system of forming stimuli-responsive colloidal clusters by exploiting the strongly temperature dependent properties of the grafted polymers.

Received 14th March 2016,  
Accepted 24th March 2016

DOI: 10.1039/c6py00450d

www.rsc.org/polymers

## Introduction

The self-assembly behavior of relatively simple colloidal particles such as spheres, rods and platelets into (liquid) crystals has provided fundamental insight into self-organization mechanisms on atomistic and molecular length scales.<sup>1–5</sup> However, these rather simple colloidal analogues of atoms and molecules are clearly not suitable as model systems for more complex assembly processes that lead to sophisticated (biological) structures such as DNA,<sup>6,7</sup> virus capsids,<sup>6,8</sup> and microtubules.<sup>9</sup> To widen the scope of colloidal self-assembly towards these intriguing examples, building blocks with anisotropic interactions and/or shape are required.<sup>10,11</sup> Especially particles that are able to form directional inter-particle bonds are promising candidates for the formation of new colloidal superstructures. These so-called patchy particles are building blocks that contain one or more specific regions, *i.e.* patches that are attrac-

tive towards similar patches on other particles. The final assembled structure is in principle determined by the number and distribution of patches over the particle surface. Computer simulations demonstrated the versatility of patchy particles and a wide variety of complex or low-coordination structures were observed as a function of the building block geometry.<sup>12–18</sup>

However, experimental realization of these systems remains a challenging task.<sup>19–24</sup> Most synthetic procedures applied to prepare these particles, such as selective deposition, surface templating, and lithography, are difficult to perform and suffer from low yields, clearly hampering systematic study of these systems.<sup>24,25</sup>

Applying wet-chemical bulk synthesis methods to produce patchy particles would greatly enhance the yield and therefore the availability of these complex building blocks. We recently showed that strictly chemically anisotropic patchy colloids are accessible *via* an emulsion-based synthesis.<sup>26</sup> The procedure relies on a heat-induced phase separation of a styrene swollen, chlorinated seed particle. During the phase separation, monomer is expelled from the seed particle in the form of a liquid protrusion, which is readily polymerized to yield solid, dumbbell-shaped colloids. Since the chlorine moieties are confined on the seed particle, the resulting colloids consist of two distinct lobes: one chlorinated, functional lobe and a non-functionalized polystyrene protrusion. In agreement with the results of Kraft *et al.*, we observed that multi-patch colloids are also obtainable *via* this synthesis route.<sup>27</sup> Merging of liquid

Van 't Hoff Laboratory for Physical and Colloid Chemistry, Debye Institute for NanoMaterials Science, Utrecht University, Utrecht, The Netherlands.

E-mail: w.k.kegel@uu.nl, bas.van.ravensteijn@gmail.com

† Electronic supplementary information (ESI) available: IR and XPS analysis of chlorinated particles, TEM analysis of dumbbell-shaped colloids and their two-patch analogues, comparing ATRP initiating capacity of chlorinated and brominated colloids, light microscopy images of salt induced clustering, verification of specificity of attraction between p(NIPAM) grafted patches, DLS measurements of p(NIPAM) grafted particles as function of temperature. See DOI: 10.1039/c6py00450d

protrusions of multiple dumbbells before polymerization yields particles with two or more chlorinated patches. The orientation between these patches is well-defined and reproducible.<sup>27</sup> The asymmetric distribution of surface chlorine groups allows for site-specific surface modifications, for example by Click Chemistry.<sup>26</sup> This orthogonal functionalization method enables us to introduce virtually any desired molecule onto the surface of the reactive patch, providing means to extensively tune inter-particle patch interactions.

In this paper, we further expand the synthetic utility of our chemically anisotropic colloids through combination with Surface-Initiated Atom Transfer Radical Polymerization (SI-ATRP) as the surface modification method of choice. As one of the more popular forms of controlled radical polymerizations, ATRP has proven to be extremely versatile for the preparation of well-defined polymers. Monodisperse polymers with controlled topology and functionality are accessible through polymerization of a wide variety of (functional) monomers.<sup>28–30</sup>

The beneficial hallmarks of ATRP are easily extendable to heterogeneous systems, such as (metallic) nanoparticles, colloids or even macroscopic surfaces, by immobilizing ATRP initiators on the surfaces of these objects.<sup>31,32</sup> Conducting an ATRP reaction in this situation yields particles with well-defined polymer brushes created *via* a *grafting-from* approach. Contrary to the *grafting-to* approach, where functional polymers are directly coupled to an activated surface, *grafting-from* ensures controlled growth of the polymer brush by continuous attachment of monomers to the developing immobilized polymer. Therefore, this immobilization route yields dense brushes of uniform thickness.

The chemical anisotropy of our dumbbell-shaped particles offers the possibility to locally functionalize the particles with ATRP initiators. The subsequent ATRP reaction yields particles that are only partially covered with end-tethered polymers. By tuning the initial geometry of the dumbbells as well as the grafting time, colloidal particles with tunable Janus balance are prepared.

Site-specific tethering of polymers using ATRP was previously reported by Okubo and co-workers.<sup>33–35</sup> Their procedure started from an oil-in-water emulsion of which the oil phase contained two types of polymers. One of these polymers was functionalized with ATRP initiators. Upon evaporation of the oil phase, the two polymers phase-separated into a micron-sized spherical Janus particle containing a reactive patch decorated with ATRP initiators, allowing for site-specific polymer grafting.

Compared to the solvent evaporation method, our procedure yields particles that are almost an order of magnitude smaller. These small dimensions are not accessible with the procedure of Okubo and co-workers, since it requires the formation of emulsions with very small droplets of the dispersed phase. These highly curved droplets are associated with a large pressure differences between the interior and exterior of the droplet and are therefore not stable. Being able to produce these partially grafted colloids in the colloidal, and therefore Brownian regime, extends their use as building blocks in (self-)assembly studies.

Furthermore, the procedure we report here is not limited to one-patch particles only. As mentioned before, multi-patch particles can be synthesized by merging of the liquid protrusions of multiple dumbbells. Functionalizing these patches allows for grafting of polymers from the particles on multiple well-defined regions, further underlining the versatility of our approach.

Being able to localize the polymer brush on specific regions on the particles allows for the introduction of directional interactions between the building blocks. Geometrically confined colloidal clusters were obtained by exploiting the fact that these particles are only partially sterically stabilized. Dispersing the grafted dumbbells in a high salt medium induces a directional interaction between the bare, non-grafted lobes.

Finally, we briefly explore the formation of stimuli-responsive colloidal clusters in this system by exploiting the temperature dependent solubility of the grafted poly(*N*-isopropylacrylamide) (p(NIPAM)) polymers.<sup>36–38</sup>

## Experimental

### Materials

Styrene (St, 99%), divinylbenzene (DVB, 55% mixture of isomers, tech. grade), 4-vinylbenzyl chloride (VBC, ≥90%, tech. grade), 3-butynyl 2-bromoisobutyrate (97%), *N*-isopropylacrylamide (NIPAM, 97%), copper bromide (Cu(I)Br, 98%), and *N,N,N',N',N''*-pentamethyldiethylenetriamine (PMDETA, 99%) were obtained from Sigma-Aldrich. Hydroquinone (99%) was purchased from Riedel-de Haën. Sodium azide (NaN<sub>3</sub>, 99%) from VWR was used. Sodium dodecyl sulfate (SDS) and sodium bromide (NaBr, ≥99%) were obtained from BDH. Potassium persulfate (KPS, >99% for analysis), sodium bisulfite (NaHSO<sub>3</sub>, ACS reagent), azobis(isobutyronitrile) (AIBN, 98%) and dimethyl sulfoxide (DMSO, 99.7%) were purchased from Acros Organics. Methanol (MeOH, exceeds ACS specifications) was obtained from J.T. Baker. Sodium chloride (NaCl, ACS reagent, ≥99.5%) was purchased from Merck. All chemicals were used as received. The water used throughout all of the syntheses was purified using a Milli-Q water purification system.

### Synthesis of chlorinated seed particles (CPs-Cl)

Cross-linked polystyrene particles (CPs) were synthesized using a standard emulsion polymerization method described in literature.<sup>26,27</sup> A 500 mL round-bottom flask equipped with magnetic stir bar was placed in an oil bath at 80 °C. Water (200 mL) was charged into the reactor and allowed to reach the bath temperature. Styrene (21.15 g), DVB (0.635 g), and SDS (0.25 g) dissolved in water (50 mL) were added. The complete mixture was allowed to heat up to the temperature of the bath. Finally, the addition of KPS (0.39 g dissolved in 37.5 mL water) initiated the polymerization. The reaction was allowed to continue for 24 h at 80 °C. The resulting latex had a solid content of 7% (measured gravimetrically). The obtained particles had a

radius of 125 nm with a polydispersity of 3.8% as determined with transmission electron microscopy (TEM).

The synthesized particles were used as seeds in the second step, in which chlorine groups were introduced at the colloidal surface.<sup>26,39</sup> Crude seed dispersion (CPs, 25 mL) and water (10 mL) were introduced into a 50 mL round-bottom flask equipped with a magnetic stir bar. The dispersion was degassed with nitrogen for 30 min. Subsequently, a mixture consisting of VBC (1 mL) and DVB (20  $\mu$ L) (CPs-Cl-100) or VBC (0.75 mL), styrene (0.25 mL) and DVB (20  $\mu$ L) (CPs-Cl-75) was added under inert atmosphere. The seeds were swollen for 1 h at 30 °C, after which the temperature was raised to 60 °C. When this temperature was reached, KPS (0.04 g) and NaHSO<sub>3</sub> (0.03 g) dissolved in water (2.5 mL) were added. The reactions were allowed to run for 4 h. The particles were washed by centrifugation and redispersion in water. The solid content of the resulting dispersions was adjusted to 5%.

Using dynamic light scattering (DLS), a hydrodynamic particle radius of 155 nm and polydispersity index (PDI) of 0.029 was measured for CPs-Cl-100, while a hydrodynamic radius of 150 nm and PDI of 0.015 was obtained for CPs-Cl-75.

The presence of the chlorine groups was confirmed for both types of chlorinated seeds using Fourier transform infrared spectroscopy (FT-IR, ATR; 1266 cm<sup>-1</sup>) and X-ray photoelectron spectroscopy (XPS; *E*<sub>b</sub> [eV]: 200, 270).

#### Synthesis of dumbbells-shaped colloids based on chlorinated seeds (DB-Cl)

The spherical chlorinated seed particles were converted to anisotropic colloids using a previously reported method.<sup>26,27,40</sup> SDS (84 mg) was introduced into a 25 mL elongated reactor tube containing a magnetic stir bar. To this tube, chlorinated seeds (CPs-Cl-100 or CPs-Cl-75, 2.5 mL, solid content = 5%) and water (2.5 mL) were added. The particles were swollen for 48 h with styrene containing 3 vol% DVB. A swelling ratio, here defined as the mass of added monomer divided by the total mass of polymer in the seed dispersion, of 3 was used for CPs-Cl-100, while a swelling ratio of 10 was applied for CPs-Cl-75.

After this swelling period, both dispersions were heated at 80 °C for 2 h, causing the formation of a liquid protrusion at the surface of the seed particles. After the 2 h period, the dispersions were allowed to cool to room temperature.

To convert the formed liquid protrusion to a solid polystyrene lobe, AIBN (4.8 mg) dissolved in styrene (230  $\mu$ L) was added, as well as 0.5 mL of a hydroquinone solution (46 mg in 50 mL water). Hydroquinone was added to prevent polymerization in the aqueous phase. The reactions were allowed to continue for 24 h at 80 °C. The resulting particles were washed using centrifugation and redispersion in water to remove unwanted aggregates and secondary nuclei. Both washed dispersions had a solid content of 1%.

The geometric shape of the particles was investigated with TEM. The synthesis conducted with CPs-Cl-100 yielded dumbbells with protrusions smaller than the chlorinated lobe (DB-Cl-100). For CPs-Cl-75, protrusions larger than the chlorinated seed particle were obtained (DB-Cl-75). In both cases, a

small fraction of two-patch particles was observed (see Fig. 2). For both colloidal systems, IR spectroscopy was used to verify the presence of the chlorine groups (1266 cm<sup>-1</sup>).

#### Introduction of bromine ATRP initiator on DB-Cl using Click Chemistry (DB-Br)

In the first step, the chlorine groups of dumbbell-shaped colloids were substituted for azides. An aqueous dispersion containing chlorinated dumbbells (DB-Cl-100 or DB-Cl-75, 1 mL, solid content = 5%) was centrifuged. The supernatant was replaced with DMSO (5 mL) and the colloids were redispersed. NaN<sub>3</sub> (7 mg) was weighed into an elongated, 4 mL reactor tube and the DMSO dispersion was added. Dissolution of NaN<sub>3</sub> was enhanced by sonication of the reaction mixture. After complete dissolution of the azide salt, the mixture was heated to 80 °C for 24 h. After this period, the particles were washed with water to remove all excess salt. IR spectroscopy was used to verify the presence of the azide functionality (2100 cm<sup>-1</sup>) which was vital for the next reaction step.

In the second step, the newly introduced azide moieties were used to couple a brominated ATRP initiator to the reactive patch of the dumbbells.<sup>41</sup> DMSO was degassed by evacuation and refilling with nitrogen several times. Cu(I)Br (100 mg) was introduced in a separate flask under inert atmosphere and degassed DMSO (2.5 mL) was added to the copper salt. The obtained CuBr/DMSO stock solution was degassed again several times to further exclude water and oxygen from the mixture.

A dispersion containing azide functionalized dumbbells (1 mL, solid content = 5%) was transferred to DMSO (0.5 mL) by centrifugation and redispersion. The obtained DMSO dispersion was added into a Schlenk flask together with 3-butylnyl 2-bromoisobutyrate (20  $\mu$ L). The complete mixture was degassed by careful evacuation and refilling with nitrogen several times. Finally, CuBr/DMSO stock solution (0.5 mL) was added under inert atmosphere, yielding a slightly green dispersion. The mixture was stirred at room temperature for 12 h. After this period, the particles were washed with ethanol and water. IR spectroscopy revealed successful introduction of the bromine containing ATRP initiator (1732 cm<sup>-1</sup>).

#### Surface-initiated ATRP of NIPAM on DB-Br

The standard ATRP procedure for dumbbell-shaped particles with protrusions smaller than the chlorinated seed lobe (DB-Cl-100) was as follows: NIPAM (240 mg, 2 mmol) and Cu(I)Br (26 mg, 0.18 mmol) were weighed and transferred directly into an oven-dried Schlenk flask. A MeOH/H<sub>2</sub>O mixture (7 : 3, v/v) (1 mL) was added and the solution was stirred for 5 min to dissolve/disperse the NIPAM and Cu(I)Br. A light green mixture was obtained. Subsequently, PMDETA (126  $\mu$ L, 0.6 mmol) was added, which caused the appearance of a blue/green color. This mixture was degassed by evacuation and refilling with nitrogen (three cycles).

In a separate Schlenk flask, the dumbbells functionalized with ATRP initiators dispersed in a 7 : 3 (v/v) MeOH/H<sub>2</sub>O mixture (1 mL, 2 wt%) were degassed by evacuation and

refilling with nitrogen (three cycles). After degassing, the dispersion was injected into the monomer/catalyst mixture under inert atmosphere. The resulting reaction mixture was white/green.

All samples withdrawn during the ATRP reaction were directly diluted with a 7:3 (v/v) MeOH/H<sub>2</sub>O mixture and rapidly washed to quench the polymerization reaction. After 4 h, the flask was opened and the remaining reaction mixture exposed to air. Contact with air turned the samples and reaction mixture intensely blue. After washing with water, 50 mM NaHSO<sub>3</sub> solution and MeOH, a white stable aqueous dispersion was obtained. The presence of p(NIPAM) was probed using IR spectroscopy (3300 cm<sup>-1</sup>: N-H vibration, 1640 cm<sup>-1</sup>: amide I; carbonyl stretching and 1536 cm<sup>-1</sup>: amide II N-H deformation).

The ATRP procedure was slightly modified for the dumbbells with large protrusions (DB-Cl-75). NIPAM, Cu(I)Br and PMDETA were dispersed in a 1:1 (v/v) MeOH/H<sub>2</sub>O mixture instead of the previously used 7:3 (v/v) MeOH/H<sub>2</sub>O mixture. The colloids were dispersed and degassed in a 1:1 (v/v) MeOH/H<sub>2</sub>O solution containing SDS and NaBr. The concentration of SDS was equal to the critical micelle concentration, while NaBr was present in a 5 times molar excess with respect to SDS. The ATRP reaction was again started by injection of the degassed particle dispersion into the monomer/catalyst mixture.

The aforementioned modifications were required to guarantee colloidal stability at the start of the ATRP reaction by adsorption of SDS onto the surface of the colloidal particles. To counteract the negative effect that SDS has on the ATRP equilibrium by forming complexes with copper ions, NaBr was added in accordance to ref. 42.

### Characterization

Infrared (IR) spectra were obtained using a PerkinElmer FT-IR/FIR Frontier Spectrometer in attenuated total reflectance (ATR) mode. Measurements were performed on powders obtained by drying the corresponding particle dispersion.

The X-ray photoelectron spectroscopy (XPS) measurements were conducted with a Thermo Scientific K-Alpha spectrometer equipped with a monochromatic small-spot X-ray source and a 180° double-focusing hemispherical analyzer with a 128-channel detector. Spectra were obtained using an aluminum anode (Al K $\alpha$  = 1486.6 eV) operating at 72 W and a spot size of 400  $\mu$ m. Survey scans were measured at constant pass energy of 200 eV and region scans at 50 eV. The background pressure was  $2 \times 10^{-9}$  mbar and during measurement the argon pressure was  $3 \times 10^{-7}$  mbar because of the charge-compensation dual-beam source.

Transmission electron microscopy (TEM) pictures were taken with a Philips Technai10 electron microscope typically operating at 100 kV. Bright field images were recorded using a SIS Megaview II CCD camera. The samples were prepared by drying a drop of diluted aqueous particle dispersion on top of polymer coated copper grids.

Optical microscopy images were obtained using a Nikon Eclipse Ti-U inverted microscope equipped with an InfinityX scout camera. A 100 $\times$  magnification objective was used.

Dynamic light scattering (DLS) and electrophoretic mobility measurements were performed using a Malvern Zetasizer Nano instrument using highly diluted aqueous dispersions at 25 °C. The DLS measurements were taken in seven runs of 15 individual measurements in backscatter mode (173°). The sizes of the colloids are reported as Z-average diameters and the corresponding polydispersity index (PDI). These values were obtained by using the cumulant method as described in ref. 43.

For the electrophoretic mobility measurements, seven runs of at least 50 individual measurements were conducted to obtain a statistically reliable zeta ( $\zeta$ ) potential. Electrophoretic mobilities were measured in Milli-Q water. The Hückel limit of the Henry equation was used to convert the measured electrophoretic mobilities to  $\zeta$  potentials.

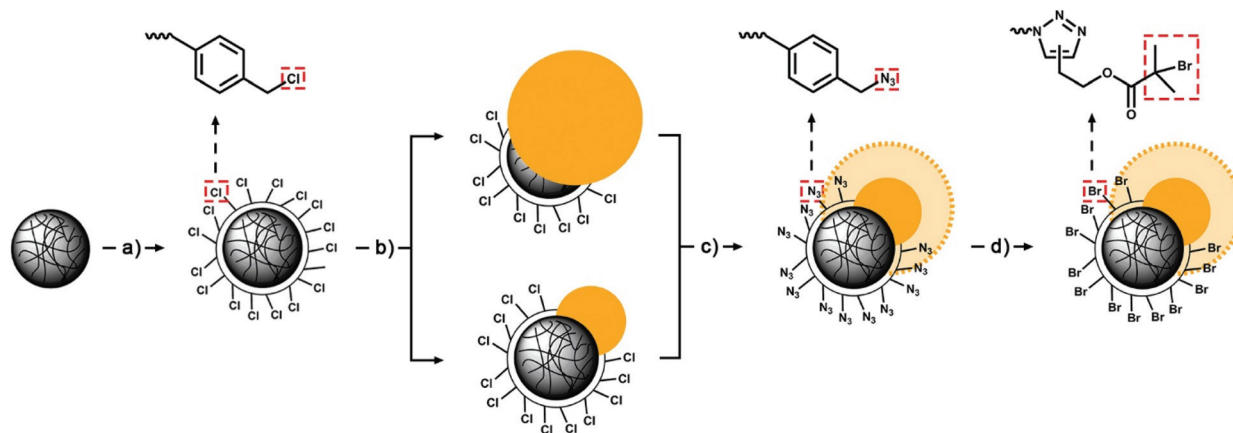
## Results and discussion

### Synthesis of ATRP initiator functionalized patchy particles

The overall synthesis procedure for chemically anisotropic dumbbell-shaped colloids capable of initiating SI-ATRP reactions is schematically depicted in Scheme 1. The first step (step a, Scheme 1) comprised a seeded-emulsion polymerization of VBC (or a mixture of VBC and styrene; see Experimental section) in the presence of cross-linked polystyrene particles. As a result, the particles were coated with a thin, chlorinated layer which provides reactive chemical handles at the surface of these particles. Introduction of the chlorine functionality was confirmed using infrared (IR) and X-ray photoelectron spectroscopy (XPS). After coating, a clear signal at 1266 cm<sup>-1</sup>, which is characteristic for the -CH<sub>2</sub>-Cl vibration, appeared in the IR spectrum. The XPS spectrum showed the appearance of signals at binding energies of 200 and 270 eV, characteristic for chlorine (ESI S1†).

These spherical, chlorinated particles (CPs-Cl) were subsequently converted into dumbbell-shaped colloids (step b, Scheme 1).<sup>26</sup> To achieve this, CPs-Cl were swollen with styrene and DVB. Swelling of the cross-linked particles induces elastic stress on the polymer network. To release this stress, the monomer swollen colloids undergo a phase separation. During this process, monomer is expelled from the seed and forms a liquid protrusion. This process is in principle spontaneous, but can be sped up significantly by heating the monomer-swollen seeds.<sup>44</sup> Polymerization of the protrusions yields solid, dumbbell-shaped colloids that consist of a functional, chlorinated lobe and a non-functional polystyrene lobe. Depending on the swelling ratio, here defined as the mass of monomer divided by the mass of polymer present in the seed dispersion, and the chemical composition of the chlorinated shell, the size ratio between chlorinated seed and protrusion is tunable. This enabled us to prepare dumbbell-shaped colloids with protrusions either smaller or larger than the chlorinated





**Scheme 1** Schematic representation of the synthesis of dumbbell-shaped colloids that consist of a non-functionalized patch (yellow) and a lobe containing ATRP initiators (Br, right). Step (a): seeded-emulsion polymerization of 4-vinylbenzyl chloride (VBC) in the presence of cross-linked polystyrene particles. Step (b): formation of dumbbell-shaped colloids which contain one chlorinated patch. Step (c): converting the surface chlorine groups on the reactive patch to azides ( $-N_3$ ) via a simple nucleophilic substitution reaction with  $NaN_3$ . Step (d): coupling of a brominated ATRP initiator to the azido-functionalized lobe by a Huisgen 1,3-dipolar cycloaddition with 3-butynyl 2-bromoisobutyrate. The chemical surface entities for each type of colloid are depicted on top of the scheme.

seed (Fig. 1a and e, respectively). This robust way to tune the overall particle geometry was confirmed by recording transmission electron microscopy (TEM) images of both types of particles. Fig. 1b and f clearly show anisotropic colloids. Protrusions were distinguished from chlorinated seed lobes by the shape of two-patch particles present in the reaction

mixture. As mentioned in the Introduction, these two-patch particles form after merging of the liquid protrusions of two individual dumbbells. This merging process is schematically depicted in Fig. 2a, together with a typical TEM image showing the obtained particle geometry (Fig. 2b). The resulting colloids contain two chlorinated patches and one central lobe that correspond to the merged protrusions. The size of the central lobe is twice that of a protrusion on a monomeric

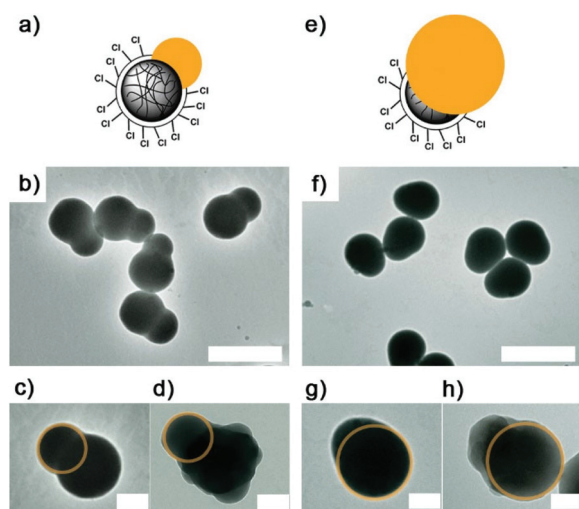


**Fig. 1** (a) Schematic representation and (b) transmission electron microscopy (TEM) image of colloidal dumbbells with a protrusion smaller than the reactive chlorinated lobe (DB-Cl-100). Scale bar = 0.5  $\mu\text{m}$ . Enlarged picture of (c) non-grafted and (d) polymer grafted colloid. The unreactive protrusion is highlighted with a yellow circle. Scale bar = 0.1  $\mu\text{m}$ . The enhanced surface roughness on the reactive patch indicates the presence of a polymer brush. (e) Schematic representation and (f) TEM image of dumbbells with a protrusion larger than the reactive chlorinated lobe (DB-Cl-75). Scale bar = 0.5  $\mu\text{m}$ . Enlarged picture of (g) non-grafted and (h) polymer grafted colloid. The unreactive protrusion is highlighted with a yellow circle. Scale bar = 0.1  $\mu\text{m}$ .

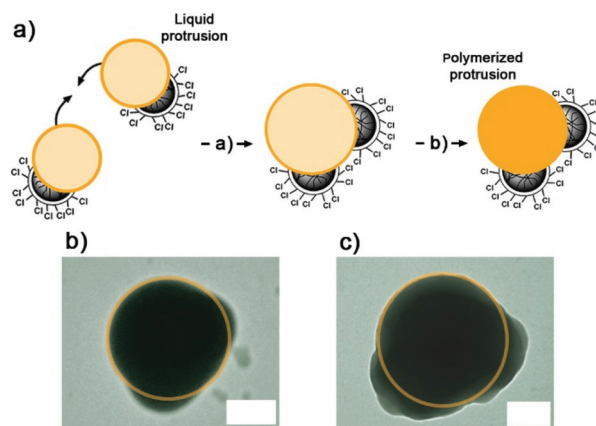


**Fig. 2** (a) Formation of colloidal two-patch particles by merging of two individual dumbbells. Dumbbells with protrusion larger than the chlorinated seed are shown (DB-Cl-75, Fig. 1f). A similar scheme is applicable to dumbbells with protrusions smaller than the seed. Step (a): merging of the liquid protrusion (light yellow) of two individual dumbbells. This yields two-patch particles with one central liquid domain and two chlorinated patches. Step (b): polymerization of the liquid central lobe to solidify the whole particle. (b) Transmission electron microscopy (TEM) image of a two-patch particle before Surface-Initiated Atom Transfer Radical Polymerization (SI-ATRP) from the reactive patches. (c) TEM image of same colloid as depicted in (b) after p(NIPAM) grafting. Scale bar = 1  $\mu\text{m}$  for all panels.

dumbbell. Therefore, by measuring the size of the central lobe of the two-patch particles reveals which lobe on a single dumbbell corresponds to the original chlorinated seed, and which to the formed protrusion (see ESI S2† for further details).

We previously showed that the chlorine groups do not migrate during protrusion formation, making that this procedure yields not only shape anisotropic, but also truly chemically anisotropic colloids.<sup>26</sup> The IR spectrum recorded after protrusion formation showed that the chlorine functionalities ( $1266\text{ cm}^{-1}$ ) were retained (Fig. 3, bottom black spectrum).

The last two steps were required to convert the surface chlorine groups of the functional lobe to the desired bromine containing ATRP initiators. The benzyl chloride functionalities can in principle also be exploited as ATRP initiators.<sup>28,30</sup> However, conducting an ATRP reaction with NIPAM as monomer in combination with the chlorinated seeds proved to be unsuccessful, since no brush formation was observed (see ESI S3†). To circumvent the inability of the benzyl chloride moieties to act as ATRP initiators, a more active bromoisobutyrate-based initiator was coupled to the reactive patch of the dumbbells.

Firstly, the chlorines were substituted by azides *via* a nucleophilic substitution with  $\text{NaN}_3$  (step c, Scheme 1). IR analysis provided confirmation of successful substitution, since a clear azide signal (Fig. 3, middle red spectrum,  $2100\text{ cm}^{-1}$ ) appeared at the expense of the chlorine vibration.

In the last step, the immobilized azides participated in a Huisgen 1,3-dipolar cycloaddition with 3-butenyl 2-bromoisobutyrate (step d, Scheme 1). This coupled the active ATRP initiator to the reactive patch of the dumbbells *via* a triazole linking moiety. The carbonyl vibration of the ester functionality ( $1732\text{ cm}^{-1}$ ) present in the initiator fragments was clearly visible in the IR spectrum of the final product (Fig. 3, top blue spectrum). Absence of the azide signal further proved successful coupling *via* the intended Click Chemistry reaction.

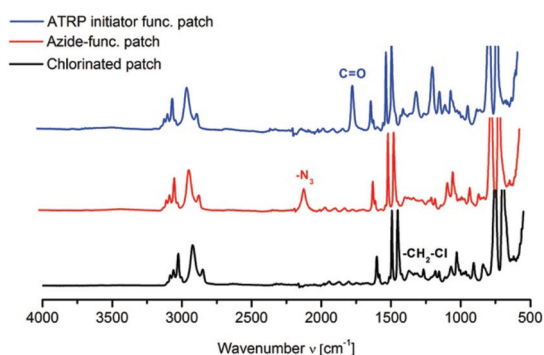


**Fig. 3** Infrared (IR) spectra of the dumbbells with a chlorinated patch (bottom, black), an azido-functionalized patch (middle, red) and the final dumbbell-shaped colloidal initiators which are site-specifically functionalized with bromine ATRP initiators. All spectra were obtained using colloids with protrusions smaller than the reactive patch (DB-Cl-100, Fig. 1a and b). Similar data were obtained for colloids with larger protrusions (DB-Cl-75, Fig. 1e and f).

TEM analysis revealed no change in particle geometry and morphology after the last two reaction steps compared to the images shown in Fig. 1.

### Site-specific brush formation *via* ATRP

With the ATRP initiators immobilized on the functionalized patch(es), subsequent polymer brush formation was attempted. *N*-Isopropylacrylamide (NIPAM) was selected as monomer and polymer brushes were introduced on both types of colloidal initiators (Fig. 1). In the upcoming section, all presented data was obtained from grafting experiments performed on dumbbells with a protrusion smaller than the reactive lobe (DB-Cl-100) (Fig. 1a). Similar results were obtained for the particles of which the protrusion was the largest lobe, with the only difference that the rate of polymerization during the grafting reaction was significantly lower. The decrease in polymerization rate was contributed to the presence of NaBr (see Experimental section).<sup>42</sup>

During the ATRP reaction, samples were withdrawn to monitor the brush formation using IR spectroscopy and dynamic light scattering (DLS).

The IR spectra show a gradual increase in intensity of the p(NIPAM) related signals ( $3300\text{ cm}^{-1}$ : N–H vibration,  $1640\text{ cm}^{-1}$ : amide I; carbonyl stretching and  $1536\text{ cm}^{-1}$ : amide II N–H deformation) over time (Fig. 4a). Since these signals are representative for the fraction of NIPAM converted to p(NIPAM) during the grafting procedure, the height of these signals is a measure for the monomer conversion ( $p$ ). Here we assumed that the signal intensity obtained after 6 h of reaction represents full conversion. Plotting the normalized carbonyl signal at  $1640\text{ cm}^{-1}$  as a function of time yields the graph plotted in Fig. 4b (black dots). This graph shows the characteristic shape of a conversion *versus* time plot for a reaction following first order kinetics. Maximum conversion was reached after approximately 90 min.

As for a conventional free radical polymerization, the rate of an ATRP polymerization can be written in terms of monomer consumption and is equal to<sup>28</sup>

$$R_p = -\frac{d[M]}{dt} = k_p[P_n^*][M] \quad (1)$$

where  $k_p$  is the rate constant for propagation,  $[P_n^*]$  the concentration of propagating radicals and  $[M]$  the monomer concentration. Integration of this equation and expressing it in terms of monomer conversion yields

$$\ln \frac{[M]_0}{[M]} = \ln \left( \frac{1}{1-p} \right) = k_p[P_n^*]t \quad (2)$$

The integration is performed under the assumption that  $[P_n^*]$  is constant over time. This assumption is in fact a hallmark for controlled radical polymerizations, since a constant number of radical species during the polymerization implies the absence of irreversible termination events. Therefore, plotting  $\ln(1/(1-p))$  *versus* time should result in a straight line

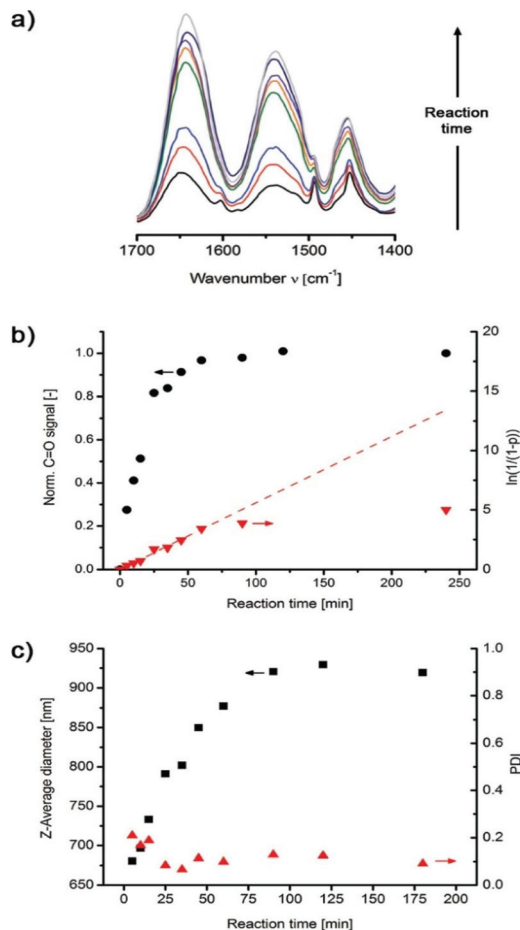


**Fig. 4** (a) Overlay of the amide vibrations ( $1640\text{ cm}^{-1}$  and  $1536\text{ cm}^{-1}$ ) observed in infrared (IR) spectra during the grafting of p(NIPAM) on dumbbell-shaped colloids with brominated initiator patches. (b) Black circles: plot of the normalized intensity of the amide vibration ( $1640\text{ cm}^{-1}$ ) (shown in (a)) versus reaction time. Red triangles: semi-logarithmic kinetic plot based on monomer conversions determined from the carbonyl vibrations. The straight line indicates the theoretical curve for a controlled radical polymerization. (c) Dynamic light scattering (DLS) results of dumbbell-shaped colloidal initiators during polymer grafting. The size of the colloids is reported as Z-average diameter (black squares). The polydispersity index (PDI) of particles is depicted by the red triangles. All data were obtained using colloids with protrusions smaller than the reactive patch (DB-CI-100, Fig. 1a and b). Similar data were obtained for colloids with larger protrusions (DB-CI-75, Fig. 1e and f).

with a slope equal to the product  $k_p[P_n^*]$  if the polymerization is controlled.<sup>28,30</sup>

This linear relationship is actually found in our grafting experiments up to almost full conversion (Fig. 4b, red triangles). Deviations from this linear relation at high conversions suggest the occurrence of termination reactions near the end of the polymerization. Due to the low monomer concentration at this stage of the reaction, chain growth is slowed down significantly and side reactions, such as termination events, take over.

Although the linear trend we find in this semi-logarithmic kinetic plot suggest a controlled polymerization up to high

monomer conversion, claiming full molecular control is not possible based on solely these data. The molecular weight evolution as function of time is required to exclude chain transfer reactions as well. However, for the modification of particles with polymer brushes, the exact molecular details are less crucial and therefore not completely investigated here.

The estimated conversion data agrees nicely with the DLS results. The hydrodynamic diameter (Fig. 4c, black squares) of the colloids increased gradually over time from 670 to approximately 900 nm. Clearly, particle size is directly coupled to the monomer conversion. This gives us a method to tune the thickness of the polymer brush by varying the grafting time. One must note that the reported values for the hydrodynamic dimensions are only indicative for the actual particle size, since the raw DLS data were converted to sizes by applying a model which assumes spherical particle geometry.

The polydispersity index (PDI, Fig. 4c, red triangles) is rather high ( $\approx 0.2$ ) at the beginning of the polymerization. As the grafting reaction proceeded, the PDI dropped and colloidal stability increased. This effect was probably caused by the increase in steric repulsion between the p(NIPAM) grafted colloids with increasing length of the immobilized polymers.

As a final analysis technique, TEM was used to obtain visual evidence for successful polymer grafting. TEM images of particles obtained after short grafting times are shown in Fig. 1d and h. These pictures clearly show irregular surface features on the reactive lobe of the dumbbells, caused by the collapsed polymer brushes. The irregular appearance of the polymers is caused by drying the samples to make them suitable for TEM analysis. The protrusions, highlighted with the yellow circles in Fig. 1d and h, which did not contain any ATRP initiators, remained smooth after brush formation. This clearly indicates the absence of end-tethered polymers at these unreactive domains of the dumbbells, implying localized polymer grafting on the reactive patches only.

Exploiting colloidal particles with two bromoisobutyrate functionalized patches as colloidal initiators, yields particles with two textured patches (Fig. 2c). As for the dumbbell-shaped colloids, the polymers are selectively tethered to the reactive sites of the colloidal particles, showing that our method can be extended to particles with more than one patch. The two-patch particles can in principle be isolated using density gradient centrifugation to obtain a dispersion containing solely these higher order patchy particles.<sup>27</sup>

Together with the results obtained from IR spectroscopy and DLS measurements, which show that the particles consisted partially out of p(NIPAM) and grew during brush formation, we concluded that site-specific polymer grafting on patchy colloidal particles was successful.

### Finite-sized cluster formation of partially grafted dumbbells

To form well-defined, finite-sized colloidal clusters, particles need to bind in a directional fashion and the clustering should be self-limiting. In practice, this translates to building blocks which carry small attractive patches. Forming predominately patch-patch interaction guarantees the directionally,



while the small dimensions limit the number of these bonds that can be formed.

For our dumbbell-shaped colloids this implies that the smallest lobe of the particles should be made attractive towards the small lobes on other particles. Since we prepared partially grafted dumbbells in which either the bare protrusion or the polymer grafted seed are the lobes with the smallest dimensions, we envisioned two different routes towards finite-sized colloidal clusters based on the partially p(NIPAM) grafted colloids (Scheme 2).

The first route relies on generating attractions between the small, bare protrusions (Fig. 1d) by the addition of salt (Scheme 2a). Upon raising the ionic strength of the aqueous solvent, the bare lobes will become attractive to other bare lobes due to screening of the electrostatic repulsion. The large polymer grafted parts of the dumbbells will remain stable through steric stabilization provided by the grafted polymer brush. Upon formation of colloidal bonds, the smooth protrusions are shielded by the hairy p(NIPAM) lobes guaranteeing a limited number of bonds per particle. This approach is not

suitable for the particles depicted in Fig. 1h. In this case, the smooth protrusions are simply too large. The small, hairy lobes cannot induce sufficient directionality into the system, leading to the formation of large ill-defined clusters if these large protrusions are attractive towards each other.

Secondly, small colloidal clusters could in principle be formed by exploiting the thermo-responsive properties of the grafted p(NIPAM) polymers (Scheme 2b). At room temperature, the grafted p(NIPAM) hairs are hydrophilic and extend into the aqueous solution. However, heating above the lower critical solution temperature (LCST) turns the p(NIPAM) polymers hydrophobic.<sup>45</sup> Patches containing these hydrophobic brushes attract each other. If the system is cooled down below the LCST again, the effective attraction between the particles vanishes and the formed clusters/aggregates disassemble spontaneously. This strategy will be applicable to the dumbbells which have a p(NIPAM) patch smaller than the bare protrusion (Fig. 1h).

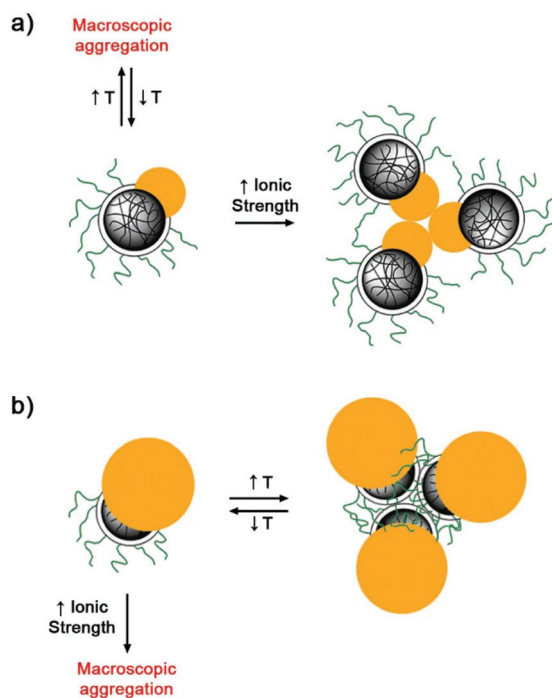
For both formation pathways we expect colloidal analogues of micelles to form, where the attractive patches are oriented to the center of the cluster. These attractive patches will be shielded by the larger lobes which reside at the outer rim of the assembly.<sup>22</sup>

In the upcoming sections, the feasibility of both formation strategies will be discussed.

### Salt-induced cluster formation

As briefly mentioned before, the addition of salt might induce a directional interaction between the bare lobes of the partially grafted dumbbells shown in Fig. 1d. For this approach to be successful, electric charges on the protrusions are required. Addition of salt screens the surface charges and interactions between the polystyrene protrusions are dominated by hydrophobic and/or van der Waals attractions. This interaction occurs specifically between the bare lobes of the particles as the polymer grafted lobe is sterically stabilized by the grafted p(NIPAM) chains, even at high ionic strengths. To ensure this stabilization, all the clustering experiments were conducted below the LCST of p(NIPAM). At these temperatures p(NIPAM) behaves as a neutral, hydrophilic polymer which extends into the continuous aqueous medium.

However, the presence of charges on the protrusions might be unexpected with the synthesis procedure in mind. No ionic monomers or initiators were used in the formation of these additional lobes. Despite this fact, the observed colloidal stability of the dumbbell-shaped particles suggests that these hydrophobic domains should be stabilized and the most probable option is the presence of surface charges. These charges on the protrusions most probably originate from the adsorption of surfactants (SDS) during formation of the liquid protrusions. This phenomenon was previously reported by Mock *et al.* who used surfactant adsorption to their advantage for the preparation of dumbbells with positively charged protrusions through the use of a cationic surfactant during the particle formation reactions.<sup>46</sup>



**Scheme 2** Routes towards finite-sized colloidal clusters composed of partially grafted dumbbell-shaped particles. (a) Starting from dumbbell-shaped particles with protrusions (yellow) smaller than the reactive chlorinated patch (DB-Cl-100), dumbbells with large p(NIPAM) (green hairs) domains are prepared via Surface-Initiated Atom Transfer Radical Polymerization (SI-ATRP). The protrusions become sticky by an increase in the ionic strength. The polymers grafted on the large patch provide steric stabilization, leading to directionality in the aggregation process. (b) Starting from dumbbells with protrusions larger (yellow) than the reactive patch (DB-Cl-75), dumbbells with small p(NIPAM) patches are accessible. These small p(NIPAM) lobes can induce thermo-reversible directional bonding between the colloids. For both routes, the small patches are made attractive to prevent macroscopic aggregation.



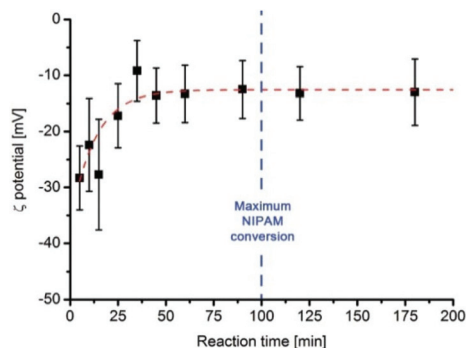


**Fig. 5** Zeta ( $\zeta$ ) potential of dumbbell-shaped colloids as function of the p(NIPAM) grafting time. The vertical, blue line represents the time at which maximum NIPAM conversion is reached (see Fig. 4b).

The presence of charges on the protrusions was confirmed using electrophoretic mobility measurements as function of the p(NIPAM) grafting time. For a charged spherical particle grafted with neutral polymers one expects the zeta ( $\zeta$ ) potential to decrease with increasing brush thickness due to an outwards shift of the hydrodynamic shear plane.<sup>47–49</sup> Based on this argument, the potential should vanish if the polymer brush becomes sufficiently long. Fig. 5 shows the  $\zeta$  potential evolution as function of the grafting time. After approximately 50 minutes of p(NIPAM) grafting, the potential levels off at  $-12$  mV. At this point, both the NIPAM conversion and the hydrodynamic radius did not reach their maximum values yet (Fig. 4). Evidently, further growth of the polymer brush does not lower the absolute value of the potential anymore. This is a strong indication that the charges present on the seed particles are not contributing anymore to the overall  $\zeta$  potential. The residual  $-12$  mV should therefore originate from charges present on the protrusions.

To investigate if the formation of small colloidal assemblies upon increasing the salt concentration was indeed feasible, partially p(NIPAM) grafted colloids (Fig. 1d) were dispersed in a 100 mM NaCl solution and subsequently analyzed with optical microscopy. This analysis revealed the presence of single particles as well as small colloidal clusters. Fig. 6 shows a few typical examples of observed clusters together with a schematic representation of dumbbell orientations inside these assemblies.

These clusters were absent in aqueous solution containing no additional salt (see ESI S4, Fig. S4a and b†), confirming that the stickiness of the colloids was indeed triggered by an increase in ionic strength.

Furthermore, the fact that we observed the formation of finite-sized colloidal clusters is strong evidence that these assemblies are formed by attraction between the smaller, smooth protrusions. Dispersing partially grafted particles with large bare, non-grafted protrusions in high ionic strength media led to the formation of large undefined clusters in agreement with our previously stated hypothesis. In contrast to the particles with a small bare protrusion, the dominating

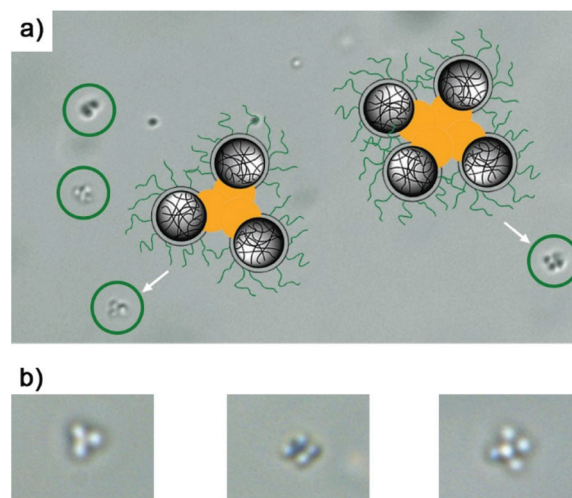


**Fig. 6** (a) Finite-size colloidal clusters observed with optical microscopy after introducing dumbbell-shaped colloids with p(NIPAM) grafted patches larger than the protrusion in a high ionic strength medium. The speculated internal structure of the clusters is illustrated by schematic representations, where the p(NIPAM) grafted lobes are depicted in grey and the bare protrusions in yellow. (b) Enlarged view of the colloidal clusters with 3, 4 or 5 individual dumbbells.

inter-particle attractions are not localized on the smaller lobes of the particles. Therefore, there is no constraint on the size of the forming aggregates (ESI S4, Fig. S4c and d†).

The formed clusters were robust. Upon dilution, the assemblies remained intact (see ESI S5†). This suggests that the high ionic strength conditions (100 mM) under which these clusters were formed, force the particles in a primary (van der Waals) minimum of which the particles can no longer escape.

### Temperature induced cluster formation

Using temperature to induce attractions between the p(NIPAM) patches is a promising route towards the reversible formation of finite-sized colloidal clusters. In principle, the partially grafted dumbbells depicted in Fig. 1h offers us the building blocks to form these dynamic clusters.

Before we employ the partially p(NIPAM) grafted dumbbells for the temperature-induced aggregation study, we would like to confirm that the interactions between the p(NIPAM) grafted patches are specific. The p(NIPAM) patches should not be attracted to the non-functionalized lobes of the dumbbells, since in that case, the directionality of the attractions is lost, which will undoubtedly result in macroscopic aggregation. At first sight, this specificity might not be apparent. Above the LCST, p(NIPAM) turns hydrophobic. The non-grafted protrusions consist of polystyrene and are therefore also hydrophobic, implying that protrusion–p(NIPAM) interactions cannot be ruled out *a priori*.

To investigate if patches with p(NIPAM) brushes would specifically bind to each other above the LCST, the following experiment was designed: spherical polystyrene colloids grafted with a p(NIPAM) brush were mixed with bare, non-

functionalized polystyrene particles. These bare colloids were significantly larger than the p(NIPAM) grafted particles, which enabled us to distinguish both types of colloids with optical microscopy. This way we prevented the use of dye molecules or other markers, which could influence the inter-particle interactions. By using this set of particles we effectively separated the p(NIPAM) patch and bare polystyrene protrusion of one dumbbell-shaped particle. By heating a mixed dispersion containing these two types of colloids we could probe which inter-particle bonds were formed preferentially. The complete synthesis and experimental set up can be found in ESI S6.†

Upon heating a dispersion containing both types of particles, small clusters started to appear (see ESI S6, Fig. S6†). Examining the clusters in more detail revealed that the formed aggregates consisted of only the smaller, p(NIPAM) grafted colloids. The non-functionalized particles were still dispersed and did not participate in cluster formation. This result indicated that above the LCST, the formation of p(NIPAM)–p(NIPAM) contacts is more favorable than p(NIPAM)–polystyrene bonds. Extrapolating this to dumbbell-shaped colloids which are partially grafted with p(NIPAM), it should be possible to induce site-specific, thermo-reversible, directional interactions between these particles.

Despite the distinct binding specificity observed between the p(NIPAM) covered particles/patches, we found that upon heating a dispersion of dumbbells with small p(NIPAM) grafted domains (Fig. 1h) above the LCST no clusters were formed. The particles remained dispersed and showed no signs of aggregation, indicating insufficient mutual attraction. Addition of salt to screen the charges present on the particles did not lead to aggregation either.

A possible explanation for the absence of attraction between the particles is that the molecular weight of the grafted p(NIPAM) is too low to undergo a significant coil-to-globule transition upon crossing the LCST. The existence of a critical molecular weight required to induce a thermo-response was previously reported in literature.<sup>50</sup> Reliable estimation of the molecular weight of the grafted polymers, and therefore comparison with literature, is difficult, since the number of ATRP initiators on the reactive patches is unknown. This information is required, because the molecular weight of the formed polymers in ATRP is set by the ratio between monomer concentration and number of initiating species.<sup>28,30</sup>

However, if we assume a high grafting density (0.25–1 chain(s) per nm<sup>2</sup>) and a NIPAM conversion of 10%, as measured with IR spectroscopy, molecular weights on the order of 10<sup>4</sup> g mol<sup>−1</sup> are found for the colloids shown in Fig. 1h. Consistent with the findings of Plunkett *et al.*, grafted p(NIPAM) polymers with molecular weights ranging between approximately 1–5 × 10<sup>4</sup> g mol<sup>−1</sup> should not show a strong temperature response.<sup>50</sup> Furthermore, experimental results obtained for spherical colloidal ATRP initiators which resemble the reactive patches of our dumbbells, confirm that the degree of brush collapse is directly related to the thickness of the brush. We validated that colloids with thin brushes do not attract each other above the LCST of p(NIPAM) (see ESI S7†). The lack of attraction strongly

suggests the absence of a coil-to-globule transition for these short polymers.

Because of this critical molecular weight requirement, slightly longer polymers were grafted onto the reactive patches of these dumbbells by simply adding more monomer to the ATRP reaction or extending the grafting time. Although, thicker and therefore thermo-responsive brushes were obtained, no finite-sized clusters were formed upon heating a dispersion containing these colloids. Instead macroscopic aggregates were obtained, indicating loss of bond directionality (see ESI S8, Fig. S10†).

TEM analysis of the grafted particles aided in rationalizing the observed macroscopic aggregation (Fig. 7). The well-defined geometric ratio between attractive and non-attractive patches of the original chlorinated colloidal dumbbells was completely lost during or after the grafting of p(NIPAM). Since relatively high molecular weight p(NIPAM) polymers were required for a convincing thermo-response, the size of the attractive patch will grow to such an extent that particles with relatively large attractive patches resulted, even if dumbbells with a relatively small reactive patch were used as colloidal initiators. The larger attractive domains on these particles cause the aggregates to grow without limit due to the insufficient protection by the non-grafted lobes.<sup>22</sup>

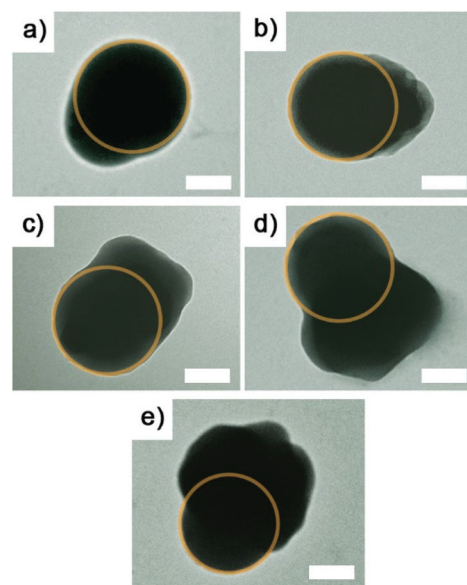


**Fig. 7** Shape evolution of dumbbell-shaped particles during a site-specific Surface-Initiated Atom Transfer Radical Polymerization (SI-ATRP) of NIPAM. The NIPAM conversion increases from panel (a) to (e). The bare protrusion is highlighted with a yellow circle. The protrusion starts out as the largest lobe of the colloids. With increasing NIPAM conversion, the dimensions of the p(NIPAM) grafted lobe increase. In panel (c) an almost shape-symmetrical particle is obtained. Prolonging the grafting time even further yield particles with p(NIPAM) patches larger than the size of the protrusion and mushroom-shaped particles are obtained (e). The irregular shape of the p(NIPAM) grafted patch is caused by drying required for the TEM analysis. Scale bar = 0.1 μm in all panels.

One way to obtain finite-size thermo-reversible clusters is to start with dumbbells that have functional patches much smaller compared to the size of the non-functionalized lobes. At this point, such extreme size ratios between seed and protrusions are not accessible based on the described emulsion-based synthesis.

### Using polymer grafting to tune Janus balance

In the previous section we observed that upon increasing the grafting time or initial NIPAM concentration, the thickness of the polymer brush may become comparable to the size of the colloidal seed particle, being on the order of hundreds of nanometers to microns. This opens the way to use the grafting reactions as a versatile tool to tune the shape and therefore Janus balance of these colloidal dumbbells.

The evolution of the particle shape as function of the grafting time for dumbbells with small reactive patches was monitored by extracting samples from the reaction mixture during the ATRP procedure. The result is shown in Fig. 7. The small functional lobe of this colloidal initiator starts off smooth (Fig. 7a). After short grafting times, the presence of polymers was observed by the formation of irregular surface features on the reactive patch (Fig. 7b). As mentioned before, the irregular appearance of the surface is caused by collapse of the grafted polymer upon preparing the TEM samples by drying the particle dispersion. The surface features slowly grow yielding nearly shape-symmetrical particles (Fig. 7c). Upon further growth, mushroom-shaped particles in which the dimensions of the p(NIPAM) grafted patch exceeds those of the bare protrusions were obtained (Fig. 7e). In this final situation, the Janus balance of the dumbbells is basically inverted; the functional lobe is now larger than the bare protrusion.

Since ATRP is a versatile polymerization technique, the described grafting reactions are not limited to the growth of p(NIPAM) brushes only. The chemical control provided by the ATRP reaction through polymerization of functional monomers is unmatched compared to those of conventional particle formation procedures, such as emulsion or dispersion polymerizations. This opens the way to tune the chemical and therefore physical characteristics of these patches to a large extend.

The tunability of the chemical characteristics is combined with simultaneously control over the particle geometry by simple variations in polymerization time or initial concentration of the grafting monomer.

## Conclusions

We showed that combining chemically anisotropic colloids with Surface-Initiated ATRP enables for site-specific grafting of p(NIPAM) brushes. The resulting dumbbells consist of a bare polystyrene lobe, and a lobe covered by end-tethered p(NIPAM) polymers. The geometric ratio between the grafted lobe and the bare lobe is tunable by the shape of the starting dumbbell as well as the grafting time.

The current system provides a new route towards the formation of colloidal clusters by exploiting the partial steric stabilization of the grafted dumbbells. Dispersing these particles in high ionic strength media induces attractions between the non-sterically stabilized lobes. Since these lobes are smaller than the p(NIPAM) covered lobes, finite-sized colloidal clusters were formed. The clusters are robust and remain intact upon lowering the ionic strength of the aqueous solvent.

Exploiting the thermo-responsive characteristics of the p(NIPAM) patches to assembly the partially grafted dumbbells into small clusters in a thermo-reversible fashion remains challenging. Although we provided clear evidence for the preferential formation of p(NIPAM)–p(NIPAM) contacts between the patches of the partially grafted dumbbells, we could not exploit this binding selectivity for the formation of finite-sized clusters. The thermo-responsiveness of grafted p(NIPAM) chains depends on the polymer length. The high molecular weight polymer required to generate a convincing temperature response results in the formation of too large p(NIPAM) patches and therefore a loss in bond directionality upon heating the system.

The large growth of the p(NIPAM) grafted domains can however be used in our advantage to tune the Janus balance of these colloidal particles. This procedure offers means to control both geometric shape and site-specific functionality in one easy grafting reaction.

The proof of principle we provide in this paper shows that combining ATRP with patchy particles is a facile way to tune both the physical and chemical characteristic of colloidal particles in a site-specific way. The reported procedure is in principle versatile and extendable to other particle geometries and polymer topologies, enabling the fabrication of even more elaborate colloidal building blocks and assembled structures.

## Acknowledgements

We would like to thank the Netherlands Organization for Scientific Research (NWO) for financial support.

## Notes and references

- 1 P. N. Pusey and W. van Megen, *Nature*, 1986, **320**, 340.
- 2 M. E. Leunissen, C. G. Christova, A.-P. Hynninen, C. P. Royall, A. I. Campbell, A. Imhof, M. Dijkstra, R. van Roij and A. van Blaaderen, *Nature*, 2005, **437**, 235.
- 3 G. J. Vroege and H. N. W. Lekkerkerker, *Rep. Prog. Phys.*, 1992, **55**, 1241.
- 4 G. J. Vroege and H. N. W. Lekkerkerker, *Philos. Trans. R. Soc. London, Ser A*, 2013, **371**, 20120263.
- 5 G. A. Vliegthart, A. van Blaaderen and H. N. W. Lekkerkerker, *Faraday Discuss.*, 1999, **112**, 173.
- 6 D. Philp and J. F. Stoddart, *Angew. Chem., Int. Ed.*, 1996, **35**, 1154.
- 7 J. D. Watson and F. H. Crick, *Nature*, 1953, **171**, 737.



- 8 J. J. McManus, A. Lomakin, O. Ogun, A. Pande, M. Basan, J. Pande and G. B. Benedek, *Proc. Natl. Acad. Sci. U. S. A.*, 2007, **104**, 16856.
- 9 A. Desai and T. J. Mitchison, *Annu. Rev. Cell Dev. Biol.*, 1997, **13**, 83.
- 10 S. C. Glotzer and M. J. Solomon, *Nat. Mater.*, 2007, **6**, 557.
- 11 A. van Blaaderen, *Nature*, 2006, **439**, 545.
- 12 Z. Zhang and S. C. Glotzer, *Nano Lett.*, 2004, **4**, 1407.
- 13 S. C. Glotzer, M. J. Solomon and N. A. Kotov, *AIChE J.*, 2004, **50**, 2978.
- 14 E. Bianchi, J. Largo, P. Tartaglia, E. Zaccarelli and F. Sciortino, *Phys. Rev. Lett.*, 2006, **97**, 168301.
- 15 F. Sciortino, A. Giacometti and G. Pastore, *Phys. Chem. Chem. Phys.*, 2010, **12**, 11869.
- 16 E. Bianchi, P. Tartaglia, E. Zaccarelli and F. Sciortino, *J. Chem. Phys.*, 2008, **128**, 144504.
- 17 G. Doppelbauer, E. Bianchi and G. Kahl, *J. Phys.: Condens. Matter*, 2010, **22**, 1.
- 18 E. Mani, E. Sanz, S. Roy, M. Dijkstra, J. Groenewold and W. K. Kegel, *J. Chem. Phys.*, 2012, **136**, 144706.
- 19 Y. Wang, Y. Wang, D. R. Breed, V. N. Manoharan, L. Feng, A. D. Hollingsworth, M. Weck and D. J. Pine, *Nature*, 2013, **491**, 51.
- 20 Q. Chen, J. K. Whitmer, S. Jiang, S. C. Bae, E. Luijten and S. Granick, *Science*, 2011, **331**, 199.
- 21 Y. Wang, A. D. Hollingsworth, S. K. Yang, S. Patel, D. J. Pine and M. Weck, *J. Am. Chem. Soc.*, 2013, **135**, 14064.
- 22 D. J. Kraft, R. Ni, F. Smallenburg, M. Hermes, K. Yoon, D. A. Weitz, A. van Blaaderen, J. Groenewold, M. Dijkstra and W. K. Kegel, *Proc. Natl. Acad. Sci. U. S. A.*, 2012, **109**, 10787.
- 23 J. R. Wolters, G. Avvisati, F. Hagemans, T. Vissers, D. J. Kraft, M. Dijkstra and W. K. Kegel, *Soft Matter*, 2015, **11**, 1067.
- 24 G.-R. Yi, D. J. Pine and S. Sacanna, *Phys.: Condens. Matter*, 2013, **25**, 193101.
- 25 A. B. Pawar and I. Kretschmar, *Macromol. Rapid Commun.*, 2010, **31**, 150.
- 26 B. G. P. van Ravensteijn, M. Kamp, A. van Blaaderen and W. K. Kegel, *Chem. Mater.*, 2013, **25**, 4348.
- 27 D. J. Kraft, W. S. Vlug, C. M. van Kats, A. van Blaaderen, A. Imhof and W. K. Kegel, *J. Am. Chem. Soc.*, 2009, **131**, 1182.
- 28 K. Matyjaszewski, *Macromolecules*, 2012, **45**, 4015.
- 29 K. Matyjaszewski and N. V. Tsarevsky, *Nat. Chem.*, 2009, **1**, 276.
- 30 K. Matyjaszewski and J. Xia, *Chem. Rev.*, 2001, **101**, 2921.
- 31 C. M. Hui, J. Pietrasik, M. Schmitt, C. Mahoney, J. Choi, M. R. Bockstaller and K. Matyjaszewski, *Chem. Mater.*, 2014, **26**, 745.
- 32 S. Edmondson, V. L. Osborne and W. T. S. Huck, *Chem. Soc. Rev.*, 2004, **33**, 14.
- 33 T. Yamagami, Y. Kitayama and M. Okubo, *Langmuir*, 2014, **30**, 7823.
- 34 T. Tanaka, M. Okayama, H. Minami and M. Okubo, *Langmuir*, 2010, **26**, 11732.
- 35 T. Takuya, M. Okayama, Y. Kitayama, Y. Kagawa and M. Okubo, *Langmuir*, 2010, **26**, 7843.
- 36 M. Zhang, L. Liu, H. Zhao, Y. Yang, G. Fu and B. He, *J. Colloid Interface Sci.*, 2006, **301**, 85.
- 37 J. N. Kizhakkedathu, R. Norris-Jones and D. E. Brooks, *Macromolecules*, 2004, **37**, 734.
- 38 T. Wu, Y. Zhang, X. Wang and S. Liu, *Chem. Mater.*, 2008, **20**, 101.
- 39 M. K. Maurer, I. K. Lednev and S. A. Asher, *Adv. Funct. Mater.*, 2005, **15**, 1401.
- 40 D. J. Kraft, J. Groenewold and W. K. Kegel, *Soft Matter*, 2009, **5**, 3823.
- 41 B. S. Sumerlin, N. V. Tsarevsky, G. Louche, R. Y. Lee and K. Matyjaszewski, *Macromolecules*, 2005, **38**, 7540.
- 42 V. L. Teo, B. J. Davis, N. V. Tsarevsky and P. B. Zetterlund, *Macromolecules*, 2014, **47**, 6230.
- 43 J. C. Thomas, *J. Colloid Interface Sci.*, 1987, **117**, 187.
- 44 W. K. Kegel, D. Breed, M. Elsesser and D. J. Pine, *Langmuir*, 2006, **22**, 7135.
- 45 M. Heskins and J. E. Guillet, *J. Macromol. Sci., Pure Appl. Chem.*, 1968, **2**, 1441.
- 46 E. B. Mock and C. F. Zukoski, *Langmuir*, 2010, **26**, 13747.
- 47 T. L. Doane, C.-H. Chuang, R. J. Hill and C. Burda, *Acc. Chem. Res.*, 2012, **45**, 317.
- 48 R. J. Hill, D. A. Saville and W. B. Russel, *J. Colloid Interface Sci.*, 2003, **258**, 56.
- 49 M. R. Gittings and D. A. Saville, *Langmuir*, 2000, **16**, 6416.
- 50 K. N. Plunkett, X. Zhu, J. S. Moore and D. E. Leckband, *Langmuir*, 2006, **22**, 4259.